

Z-pole test of effective dark matter diboson interactions at the CEPC

Yu Gao^{1*} and Mingjie Jin^{1,2†}

¹ *Key Laboratory of Particle Astrophysics, Institute of High Energy Physics,
Chinese Academy of Sciences, Beijing, 100049, China and*

² *School of Physical Sciences, University of Chinese Academy of Sciences, Beijing, 100049, China*

In this paper we investigate the projected sensitivity to effective dark matter (DM) - diboson interaction during the high luminosity Z-pole and 240 GeV runs at the proposed Circular Electron Positron Collider (CEPC). The dimension-7 effective diboson operators to fermionic dark matter generate semi-visible Z decay, and high missing transverse momentum mono-photon signals that can be test efficiently at the CEPC, with a small and controllable Standard Model $\gamma\bar{\nu}\nu$ background. At the Z-pole energy, on-resonance production of Z offers a good probe into DM - γZ couplings that is less stringently tested in non-collider searches. A projected sensitivity for effective γZ coupling efficient $\kappa_{\gamma Z} < (370 \text{ GeV})^{-3}$, $(540 \text{ GeV})^{-3}$ is obtain for 25 fb^{-1} and 2.5 ab^{-1} Z-pole luminosities assuming an optimal light dark matter mass. Effective DM-diphoton coupling sensitivity $\kappa_{\gamma\gamma} < (350 \text{ GeV})^{-3}$ is also obtained for a 5 ab^{-1} 240 GeV Higgs run, and we compare the CEPC sensitivities to current direct and indirect search results.

I. INTRODUCTION

Astrophysical [1, 2] and cosmological [3][4] evidences indicate the existence of dark matter(DM) as a major component of our Universe. From a particle physics point of view, a DM candidate particle can emerge from various theories beyond the Standard Model (SM). A weakly interacting DM particle at the electroweak mass scale (WIMP) is the most popular candidate for its natural prediction of today's thermal relic matter density.

A WIMP does not necessarily interact with weak forces themselves or directly couple to SM particles. Instead, its interaction to the SM can be mediated by other new physics particles that participate in SM interactions. These SM-interacting mediators can be efficiently searched for at colliders [5, 6] and are often constrained to be massive. For heavy mediators, one can adopt the effective theory and let the dark matter obtain effective couplings to the SM particles. For instance, mediators that carry SM gauge interaction charges may induce effective DM coupling to SM gauge bosons at loop level. A model independent approach is to study general forms of high-order effective DM-SM operators and their phenomenology in indirect, direct detection and collider searches.

At colliders, effective interactions allow DM particles to be produced as missing transverse energy (MET) by in association with a mono-jet [7] or single gauge boson [8, 9] final states. The effective DM coupling gauge bosons has been actively searched for at the LHC and the strongest limits comes from the mono-photon channel [10]. Direct detection also give significant constraint on the DM effective coupling to gauge boson, particularly in effective photonic couplings due the low momentum transfer in the nucleus - DM collision process.

The proposed high luminosity runs at the future Circular Electron Position Collider (CEPC) offer a unique opportunity to DM effective couplings to the Z boson. The Z-pole runs in particular, with projected 10^9 (giga-Z) or 10^{11} (tera-Z) integrated on-shell Z luminosities, will greatly improve the probe for Z coupling to DM. Effective DM-diboson coupling to γZ , ZZ leads to resonance-enhanced production of DM and an associated photon for a DM lighter than one half of Z mass. While a mono-photon final state does not reconstruct back to the Z mass, the single photon with large transverse momentum and recoiling MET offer a clean test channel with a small SM background.

In this work, we consider the dimension-7 fermionic effective theory DM-diboson interaction to γ and Z and study the testing sensitivity at the CEPC's Z-pole and 240 GeV runs. We briefly discuss the effective operators and the induced photon spectra in Section II and III. We analyze the CEPC mono-photon signals in Section IV. Comparisons between CEPC, direct and indirect searches are given in Section V and then we conclude in Section VI.

II. EFFECTIVE DIBOSON OPERATORS

Standard Model gauge singlet DM can obtain loop-level coupling to the SM gauge bosons if they couple to heavy new physics state that are charged under SM gauge interactions. High-dimensional operators can be derived by

* gaoyu@ihep.ac.cn

† jinmj@ihep.ac.cn

integrating out the heavy states. A comprehensive list of high-dimensional operators are discussed in Ref. [12, 13]. To the lowest order, such operators would let the DM couple to one gauge boson, e.g. the electromagnetic dipole [14, 15] and anapole [16] interactions. Such interactions lead to significant direct-detection signals and hence are stringently constrained [17, 18]. Here we consider the fermionic DM-diboson effective operators of dimension-seven. With a focus on the prospect of e^+e^- collision, we only consider the electroweak gauge fields,

$$\mathcal{L}_1 = \kappa_1 \bar{\chi} \chi B^{\mu\nu} B_{\mu\nu} + \kappa_2 \bar{\chi} \chi W^{a,\mu\nu} W_{\mu\nu}^a, \quad (1)$$

where $B_{\mu\nu}$ and $W_{\mu\nu}$ are the SM $U(1)_Y$, $SU(2)_L$ field strengths (FS). Here the DM fermion χ is a Dirac SM singlet. κ is the effective coupling coefficient for each term and it is of dimension -3. After electroweak symmetry breaking the operators can be written for the physical γ, Z, W states,

$$\mathcal{L}_1 \supset \kappa_{\gamma\gamma} \bar{\chi} \chi A^{\mu\nu} A_{\mu\nu} + \kappa_{\gamma Z} \bar{\chi} \chi A^{\mu\nu} Z_{\mu\nu} + \kappa_{ZZ} \bar{\chi} \chi Z^{\mu\nu} Z_{\mu\nu} + \kappa_{WW} \bar{\chi} \chi W^{\mu\nu} W_{\mu\nu}. \quad (2)$$

Here the physical W denote only the charged components. While $\kappa_{WW} = \kappa_2$, the other coefficients are related by the rotation of Weinberg angle,

$$\kappa_{\gamma\gamma} = \kappa_1 \cos^2 \theta_W + \kappa_2 \sin^2 \theta_W, \quad (3)$$

$$\kappa_{ZZ} = \kappa_2 \cos^2 \theta_W + \kappa_1 \sin^2 \theta_W, \quad (4)$$

$$\kappa_{Z\gamma} = (\kappa_2 - \kappa_1) \sin 2\theta_W. \quad (5)$$

The κ coefficients are dimensionful and we will denote $\Lambda_{VV}^{-3} \equiv \kappa_{VV}$, $V = \{\gamma, Z\}$ for the convenience of demonstration and comparison with heavy states in new physics models that generate such terms. Note Λ^{-3} absorbs the couplings and its exact form in complete UV models would be consist of both SM and new physics couplings and/or masses. Thus Λ may not equate the heavy mediator mass(es).

The Z -pole analysis in this paper is mostly sensitive to the first two terms in Eq. 2. In comparison, effective WW couplings can be readily searched for at the LHC, esp. in s -channel W Drell-Yan and WW fusion processes, but less so at CEPC due to the charge-neutral collision in-state and a limited energy reach.

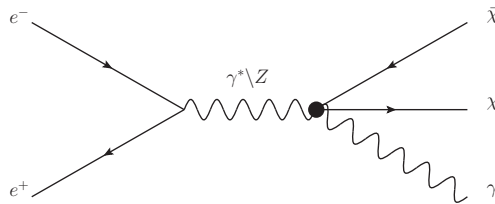


FIG. 1. DM production processes $e^+e^- \rightarrow \gamma^* Z \rightarrow \bar{\chi} \chi \gamma$ with mono- γ channel. The s -channel Z will be on-shell during Z -pole runs at the CEPC.

III. SEMI-VISIBLE Z BOSON DECAY

For a light DM mass, the effective DM γZ coupling lets the physical Z decay semi-visibly into a photon and a DM pair as illustrated in Fig. 1. This decay would contribute to the total Z width, as well as to the invisible width due to the partially invisible final state. This three-body decay rate is,

$$d\Gamma = \frac{1}{2M_Z} |\mathcal{M}|^2 d\Phi_3, \quad (6)$$

$$|\mathcal{M}|^2 = \frac{16}{3\Lambda^6} (M_Z E_\gamma)^2 (M_Z^2 - 4m_\chi^2 - 2M_Z E_\gamma), \quad (7)$$

where Φ_3 is the three-body phase-space. In the amplitude square, the χ energy E_χ is already integrated out and Eq. 7 is written in terms of the visible E_γ . The differential width can be written as,

$$\frac{d\Gamma}{dE_\gamma} = \frac{M_Z E_\gamma^2 (M_Z^2 - 4m_\chi^2 - 2M_Z E_\gamma) \sqrt{E_\gamma^2 [(M_Z^2 - 2E_\gamma M_Z - 2m_\chi^2)^2 - 4m_\chi^4]}}{12\pi^3 \Lambda^6 (M_Z^2 - 2E_\gamma M_Z)}, \quad (8)$$

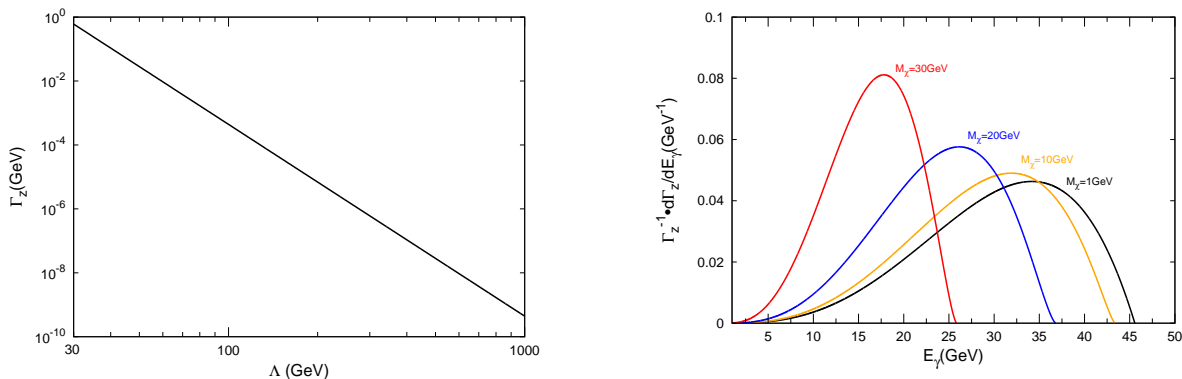


FIG. 2. Γ_Z dependence on $\Lambda_{\gamma Z}$ (left) in the low m_χ limit and the normalized photon energy spectrum $\Gamma_Z^{-1} \cdot d\Gamma/dE_\gamma$ (right) for several light DM masses with $\Lambda_{\gamma Z}$ fixed at 200 GeV.

with the minimal and maximal photon energies at 0 and $(M_Z^2 - 4m_\chi^2)/2M_Z$. Note that the photon has a hard spectrum that can be readily searched, as shown in Fig 2.

The semi-visible contribution to Z width can be a test for $\Lambda_{\gamma Z}$, as illustrated in the left panel in Fig. 2. The existing constraint on invisible Z width $\Delta\Gamma_{\text{inv}} < 2.0$ MeV at 95% CL is from LEP data [19], which corresponds to a $\Lambda_{\gamma Z} > 75$ GeV bound that is less stringent compared to the mono-photon limit.

IV. CEPC MONOPHOTON SEARCH

At the e^+e^- collider, the effective DM diboson couplings give rise to mono- γ and mono- Z signals. Both channels are sensitive probes due to a clean and identifiable SM background, if compared to hadron colliders. The mono- Z photon is favorably tested off Z -pole and has been recently studied by Ref. [11]. We focus on the monophoton signal that receives on-shell resonance enhancement at the CEPC's Z -pole energy. While $\Lambda_{\gamma\gamma}$ also contributes to this process, its contribution is not resonance enhanced. Therefore the Z -pole is a good probe $\Lambda_{\gamma Z}$ that is otherwise often subdominant in direct and indirect searches.

The mono- γ process is illustrated in Fig. 1. The DM is pair-produced in association an energetic photon, which recoils against the invisible DM pair. The photon is not forwardly (beam-line direction) enhanced, hence it leads to large photon transverse momentum (P_T) and the recoiling MET, making it a very clean search channel. With a $O(10)$ GeV photon P_T cut, the only relevant SM background channel is $e^+e^- \rightarrow \gamma\nu\bar{\nu}$, where the invisible $\nu\bar{\nu}$ splits from a virtual Z . As the total energy is capped at Z mass, the virtual $Z \rightarrow \nu\bar{\nu}$ process acquires suppression by a virtuality $\sim E_\gamma$. This background contamination can be efficiently controlled with a $P_T(\gamma)$ cut. While three neutrino flavors contribute equally to the $\gamma\nu\bar{\nu}$ background via virtual Z mediation, $\gamma\nu_e\nu_e$ has additional contribution from t -channel W exchanges.

Another background may rise from the soft e^-e^+ scattering, where a photon can be emitted and the forward-going e^\pm has a chance of escaping detection if their pseudorapidity is large. This background is however suppressed by photon P_T and can be very effectively vetoed by a single photon $P_T(\gamma)$ cut and non-observation of other detector activity [20], making it much subleading compared to $e^+e^- \rightarrow \gamma\nu\bar{\nu}$ and can be ignored in our analysis.

We use the *CalcHep* package [21] to simulate the leading-order signal and background cross-sections at CEPC Z -pole and 240 GeV runs, with basic photon pseudorapidity η and P_T cuts. Due to the cleanness in the final state, lepton flavor identification and jet reconstruction in a full detector simulation is not needed. The photon detection efficiency is near-unity [22] in the energy range of interest, and the tree-level *CalcHep* calculation should suffice. According to Ref. [22], we adopt the $|\eta(\gamma)| < 3$ cut. Then we optimize the $P_T(\gamma)$ cut between 10 GeV to 40 GeV to find the maximal sensitivity $S/\sqrt{S+B}$.

In Fig. 3, we show the photon energy $E(\gamma)$ and transverse momentum $P_T(\gamma)$ distributions for e^+e^- center of mass energy at 91.2 GeV and 240 GeV. The signal cross-section scales as $\sigma \propto \Lambda^{-6}$. It is clear that at Z -pole the signal photons have a broad P_T distribution while the background centers at low P_T and can be distinguished with a simple $P_T(\gamma)$ cut. At 240 GeV, however, the higher center of mass energy allows the Z boson to be on-shell and the $\nu\bar{\nu}$ system can have a large energy, leading a peak at high energy/ P_T end and a simple $P_T(\gamma)$ cut becomes less effective.

Table I lists the signal and background cross sections σ after a set of $P_T(\gamma)$ cut values from 15 to 40 GeV. The show-case signal cross-sections assume a light χ mass at 1 GeV and $\Lambda_{\gamma Z} = \Lambda_{\gamma\gamma} = 200$ GeV. At Z -pole, $\Lambda_{\gamma Z}$ contribution dominates. For heavier m_χ , the final state photon energy is kinematically limited and becomes softer, leading to

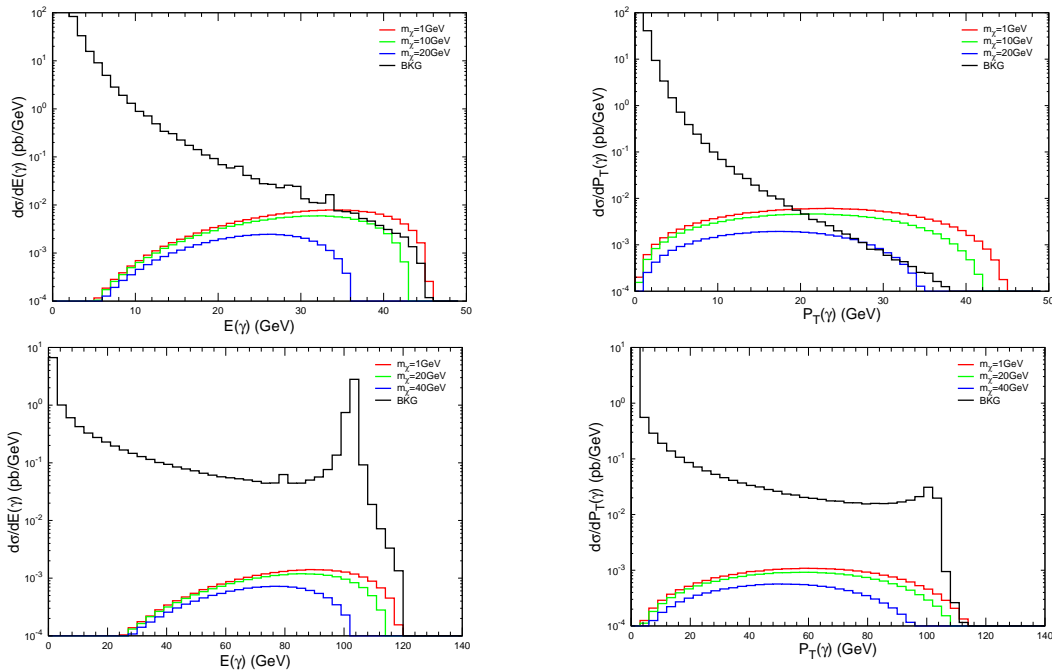


FIG. 3. Distributions of $E(\gamma)$ (left), $P_T(\gamma)$ (right) at $\sqrt{s}=91.2$ (top), 240GeV (bottom) with $\Lambda = 200\text{GeV}$ at the CEPC with several choices of m_χ . The background curve is for the irreducible SM $e^+e^- \rightarrow \gamma\nu\nu$ process.

$\sqrt{s} = 91.2\text{GeV}$			$\sqrt{s} = 240\text{GeV}$		
Cut	$\nu\bar{\nu}\gamma$	$\bar{\chi}\chi\gamma$	Cut	$\nu\bar{\nu}\gamma$	$\bar{\chi}\chi\gamma$
$P_T(\gamma)$ (GeV)	σ (fb)	σ (fb)	$P_T(\gamma)$ (GeV)	σ (pb)	σ (fb)
15	73	128	25	2.0	72
20	24	100	30	1.7	68
25*	8.6	70	35*	1.5	64
30	2.9	41	40	1.4	60

TABLE I. Cross sections of SM background and signal processes at $\sqrt{s} = 91.2$ and 240 GeV CEPC runs. Photon pseudorapidity restrict to the central region, $|\eta| < 3$. For the listed signal cross-sections, the DM mass is fixed at $m_\chi = 1\text{GeV}$ and $\Lambda_{\gamma Z} = \Lambda_{\gamma\gamma} = 200$ GeV. The $P_T(\gamma)$ cut with * is the optimized value at each energy for a low DM mass.

larger SM background and lower sensitivity to Λ . This photon would eventually vanish as m_χ approaches to the beam energy, as illustrated in Fig. 3. We choose the $P_T(\gamma)$ cut at 25 and 35 GeV for Z -pole and 240 GeV runs that optimizes the sensitivity for a low $m_\chi \sim \text{GeV}$.

The design luminosity at CEPC [23] is 25 fb^{-1} (giga-Z) and 2.5 ab^{-1} (tera-Z) at the Z -pole and 5 ab^{-1} in the high-energy 240 GeV run. We set 3σ sensitivity on $\Lambda_{\gamma Z}, \Lambda_{\gamma\gamma}$ by requiring the significance $S/\sqrt{S+B} = 3$ at the specified luminosities. S, B are the event numbers for signal and SM background channels, respectively. The result for prospective $\Lambda_{\gamma Z, \gamma\gamma}$ sensitivities are shown in Fig. 4 and later in Fig. 7. We find the Z -pole has better sensitivity on $\Lambda_{\gamma Z}$ at like luminosities $\mathcal{O}(\text{ab}^{-1})$, while 240 GeV offers better limit on $\Lambda_{\gamma\gamma}$.

V. DIRECT AND INDIRECT LIMITS

In this section we discuss the (mostly) $\Lambda_{\gamma\gamma}$ bounds from current direct and indirect search experiments. We start with direct detection. The effective diboson interaction allows the DM to scatter off nuclei via a gauge boson loop, as shown in left-panel of Fig. 5. The momentum transfer in direct detection experiments is at keV scale and the diphoton exchange dominates the scattering process. The diphoton scattering process bears similarity to Rayleigh

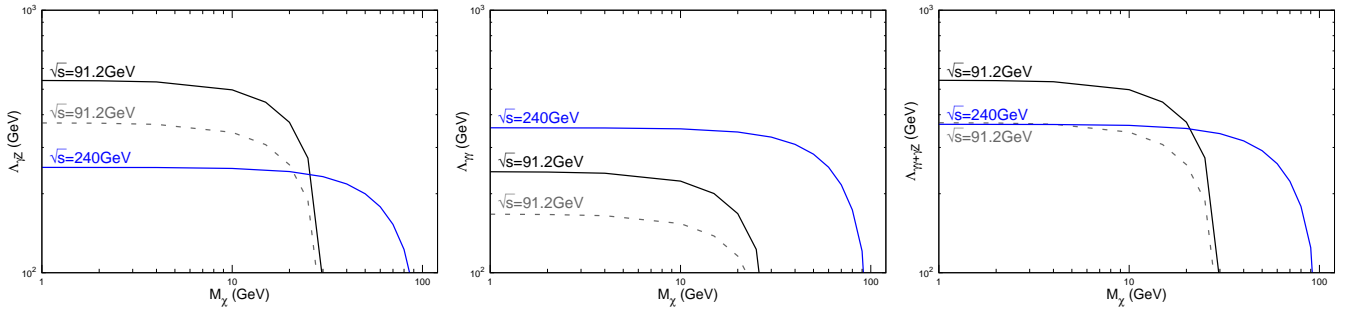


FIG. 4. The 3σ reaches in the $m_\chi - \Lambda$ plane. The gray, black and blue lines denote $\sqrt{s} = 91.2\text{GeV}$ at 25 fb^{-1} (giga-Z), 2.5 ab^{-1} and 240 GeV at 5 ab^{-1} . The left, middle and right panels assume $\Lambda_{\gamma Z}$ -only, $\Lambda_{\gamma\gamma}$ -only and $\Lambda_{\gamma Z} = \Lambda_{\gamma\gamma}$ cases. $P_T(\gamma)$ cut is at 25 (35) GeV for 91.2 (240) GeV runs that optimizes the sensitivity for a low m_χ .

scattering [24]. Following the procedure in Ref. [25], we compute the DM-nucleus scattering cross-section with,

$$\sigma_N = \frac{8\mu_A^2 \alpha^2 Z^2 Q_0^2 F_{\text{Ray}}(\bar{q})}{\pi^2 \Lambda_{\gamma\gamma}^6} \quad (9)$$

where the reduced mass $\mu_A = m_A m_\chi / (m_A + m_\chi)$, the form factor $F_{\text{Ray}}(\bar{q})$ drops with rising momentum transfer. The nuclear coherence scale $Q_0 \simeq 0.48(0.3 + 0.89A^{1/3})^{-1}\text{ GeV}$. The photon mediated scattering is enhanced by the nucleus's number of protons as Z^2 . The γZ -loop contribution is subleading due to M_Z suppression in the heavy propagator. While the $\gamma\gamma, \gamma Z$ interference diagram can be relevant for $\Lambda_{\gamma Z} \ll \Lambda_{\gamma\gamma}$, the γZ scattering calculation is currently unavailable and is important for future research. Here we only include $\Lambda_{\gamma\gamma}$ contribution in direct detection limits.

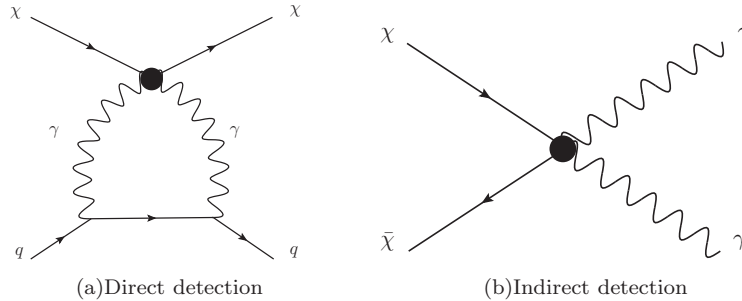


FIG. 5. Feynman diagrams for DM diphoton scattering off nucleus (left) in direct detection, and diphoton DM annihilation process (right) for indirect gamma-ray search.

A number of existing direct experiments set limits on accessible m_χ at the CEPC. We illustrate the constraints from a list of recent direct detections results on $\Lambda_{\gamma\gamma}$ in Fig. 6(a). For $m_\chi > 10\text{ GeV}$, the latest Xenon-based experiments readily set $\Lambda_{\gamma\gamma}$ limit at TeV or higher. A lower $m_\chi < 4\text{ GeV}$ would observe a sub-100 GeV $\Lambda_{\gamma\gamma}$ bound from current direct detection results, and may be more effectively searched for in future low-threshold nucleus recoil detectors.

For indirect detection, the non-relativistic cross section of DM annihilation into two photons ($\bar{\chi}\chi \rightarrow \gamma\gamma$) is dominated by $\Lambda_{\gamma\gamma}$,

$$\langle\sigma v\rangle_{\gamma\gamma} = \frac{m_\chi^4 v^2}{\pi \Lambda_{\gamma\gamma}^6}, \quad (10)$$

for m_χ below $M_Z/2$. Note the operators in Eq. 1 leads to a p -wave annihilation. $\Lambda_{\gamma Z}$ dependence only emerges in a small correction from Z mediation as part of the $\bar{\chi}\chi \rightarrow \gamma(\gamma^*/Z^* \rightarrow \bar{f}f)$ process, which is suppressed by the $f\bar{f}$ mass for virtual photon mediation and M_Z for virtual Z mediation. As a result, $\Lambda_{\gamma\gamma}$'s contribution also by far dominates over that of $\Lambda_{\gamma Z}$. In Fig. 6(b) we show the 95% CL $\Lambda_{\gamma\gamma}$ constraint from gamma ray line search at Fermi-LAT [32].

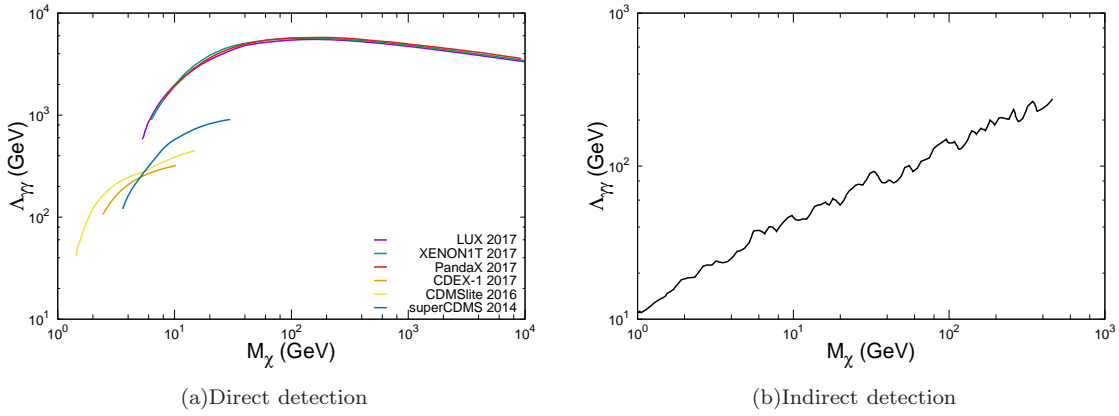


FIG. 6. Limit on $\Lambda_{\gamma\gamma}$ for m_χ from direct (left) and indirect (right) detection searches. Direct detection includes latest results from SuperCDMS [26], CDEX [27], CDMSlite [28], XENON1T [29], LUX [30] and PandaX [31] experiments. Indirect detection uses the Fermi-LAT’s monochromatic photon constraint from R3 [32] observation region.

In case of s -wave annihilation by $\bar{\chi}\gamma^5\chi A\tilde{A}$ interaction, the galactic velocity suppression $v^2 \approx 10^{-6}$ is lifted and the $\Lambda_{\gamma\gamma}$ bound improves by one order of magnitude.

Fig. 7 shows the CEPC, direct and indirect detection limits on the $\Lambda_{\gamma\gamma} - \Lambda_{\gamma Z}$ plane. The direct detection calculation only includes $\Lambda_{\gamma\gamma}$ contribution. For the indirect constraint, $\Lambda_{\gamma Z}$ contribution is small and does not cause visible shape-change in the plotted parameter range. The red, orange, pink dashed areas denote for SuperCDMS [26], CDEX [27], CDMSlite [28] bounds. The green dashed area shows the bound from XENON1T [29]\LUX [30]\PandaX [31] for their close proximity to each other. The purple line denotes Fermi-LAT constraint from R3 region [32]. The black, gray and blue lines denote for CEPC 3σ sensitivities with integrated luminosity of 2.5ab^{-1} , 25fb^{-1} at $\sqrt{s} = 91.2\text{GeV}$ and 5ab^{-1} at $\sqrt{s} = 240\text{GeV}$, corresponding to prospective 10^{11} , 10^9 Z boson and 10^6 Higgs runs. For comparison we include for ILC’s 3σ monophoton sensitivity (brown curve) with integrated luminosity of 500fb^{-1} at $\sqrt{s} = 500\text{GeV}$ [33].

While $\Lambda_{\gamma\gamma}$ can be more tightly constrained at the latest direct-detection experiments, CEPC can offer good $\Lambda_{\gamma Z}$ sensitivity in the Z -pole runs. For a low m_χ , giga- Z (tera- Z) run can probe $\Lambda_{\gamma Z}$ to 370 and 540 GeV at 3σ sensitivity. This limit is higher than the LHC 8 TeV constraints [9] and slightly lower than the 13 TeV LHC monophoton results [10].

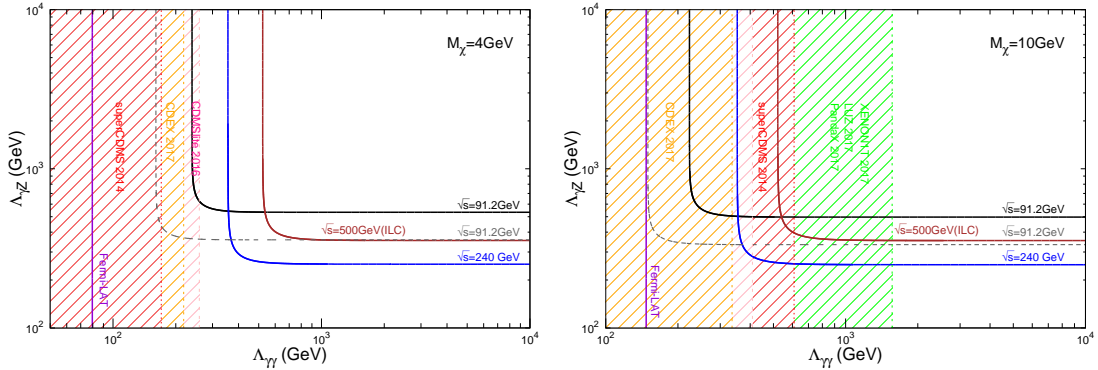


FIG. 7. limit on $\Lambda_{\gamma\gamma} - \Lambda_{\gamma Z}$ for direct, indirect and collider detection. In left(right) plot, the DM mass is $m_\chi=4(10)\text{GeV}$. The red, orange, pink and green dashed areas denote SuperCDMS, CDEX, CDMSlite and XENON1T\LUX\PandaX, respectively. The purple line denotes Fermi-LAT from R3 region in indirect detection. The black, gray and blue lines denote integrated luminosity of 2.5ab^{-1} , 25fb^{-1} at $\sqrt{s} = 91.2\text{GeV}$ and 5ab^{-1} at $\sqrt{s} = 240\text{GeV}$, corresponding to 10^{11} , 10^9 Z boson particles and 10^6 Higgs particles, respectively, where the significance reaches to 3σ and cuts are as follows: $|\eta| < 3$ and $P_T(\gamma) > 25\text{GeV}$ at $\sqrt{s} = 91.2\text{GeV}$; $P_T(\gamma) > 35\text{GeV}$ at $\sqrt{s} = 240\text{GeV}$. The brown line denotes for ILC 3σ sensitivity with integrated luminosity of 500fb^{-1} at $\sqrt{s} = 500\text{GeV}$ with cuts $10^\circ < \theta_\gamma < 170^\circ$ and $P_T(\gamma) > 50\text{GeV}$. Note that the XENON1T\LUX\PandaX limit only appears in $m_\chi=10\text{ GeV}$ case.

VI. CONCLUSION

In this work, we consider dimension-7 effective DM diboson operators and their test via the monophoton search channel at the CEPC. With a focus on the Z -pole energy, the effective DM couplings to the Z boson can be accessed at large luminosity giga- Z and tera- Z runs. A DM mass below $M_Z/2$ allows for the three-body $Z \rightarrow \bar{\chi}\chi\gamma$ monophoton final state, where the photon is energetic and it recoils against a large MET. The major SM background $e^+e^- \rightarrow \bar{\nu}\nu\gamma$ is relatively small and is under good control with a transverse photon momentum cut. We adopt optimized photon P_T cuts at 25 and 35 GeV for the Z -pole (91.2 GeV) and 240 GeV runs, and derive the 3σ sensitivity for the effective diboson couplings $\Lambda_{\gamma Z}$ and $\Lambda_{\gamma\gamma}$.

Best $\Lambda_{\gamma Z}$ sensitivity occurs at Z -pole due to on-resonance production of the Z boson, where $\Lambda_{\gamma Z}$ contribution dominates. Proposed 25 fb $^{-1}$ and 2.5 ab $^{-1}$ Z -pole luminosity runs can probe $\Lambda_{\gamma Z}$ to 370 and 540 GeV in the low DM mass limit. 240 GeV run loses sensitivity in $\Lambda_{\gamma Z}$ as the center of mass energy moves away from Z -pole and a better sensitivity in $\Lambda_{\gamma\gamma}$ is obtained instead, and at 5 ab $^{-1}$ luminosity $\Lambda_{\gamma\gamma}$ can be probed to 350 GeV. Sensitivity for variant DM mass and $\Lambda_{\gamma Z}, \Lambda_{\gamma\gamma}$ combinations are given in Figs. 4 and 7.

We compare the CEPC's sensitivities to current constraints from direct and indirect dark matter searches. Limits from the latest experiments are shown in Fig. 7. Non-collider searches can be very sensitive to $\Lambda_{\gamma\gamma}$ and give a higher than TeV $\Lambda_{\gamma\gamma}$ constraint in their optimal DM mass range. In comparison, the CEPC runs give better $\Lambda_{\gamma\gamma}$ sensitivity than direct and indirect searches at low (< 4 GeV) DM mass range, and better $\Lambda_{\gamma Z}$ sensitivity for DM masses accessible to the CEPC. Comparing to LHC monophoton searches, CEPC's $\Lambda_{\gamma Z}$ constraint is better than 8 TeV LHC bounds and less stringent than 13 TeV LHC results.

Acknowledgements

The authors thank Xiao-jun Bi and Pengfei Yin for helpful discussions. Y.G. is supported under grant no. Y7515560U1 by the Institute of High Energy Physics, Chinese Academy of Sciences. M.J. thanks the Institute of High Energy Physics, Chinese Academy of Sciences for support.

-
- [1] F. Zwicky, *Astrophys. J.* **86**, 217 (1937).
 - [2] D. Clowe, A. Gonzalez and M. Markevitch, *Astrophys. J.* **604**, 596 (2004) [astro-ph/0312273].
 - [3] D. N. Spergel *et al.* [WMAP Collaboration], *Astrophys. J. Suppl.* **170** (2007) 377 [astro-ph/0603449].
 - [4] P. A. R. Ade *et al.* [Planck Collaboration], *Astron. Astrophys.* **594** (2016) A13 [arXiv:1502.01589 [astro-ph.CO]].
 - [5] CMS Exortica summaries: <http://cms-results.web.cern.ch/cms-results/public-results/publications/EXO/index.html>
 - [6] ATLAS Exortica summaries: <https://twiki.cern.ch/twiki/bin/view/AtlasPublic/ExoticsPublicResults>
 - [7] J. Goodman, M. Ibe, A. Rajaraman, W. Shepherd, T. M. P. Tait and H. B. Yu, *Phys. Rev. D* **82**, 116010 (2010) [arXiv:1008.1783 [hep-ph]]. U. Haisch, F. Kahlhoefer and E. Re, *JHEP* **1312**, 007 (2013) [arXiv:1310.4491 [hep-ph]]. Y. Yamamoto, *PTEP* **2014**, 123B03 (2014) [arXiv:1409.5775 [hep-ph]]. D. Racco, A. Wulzer and F. Zwirner, *JHEP* **1505**, 009 (2015) [arXiv:1502.04701 [hep-ph]]. R. M. Godbole, G. Mendiratta, A. Shivaji and T. M. P. Tait, *Phys. Lett. B* **772**, 93 (2017) [arXiv:1605.04756 [hep-ph]]. F. Pobe, A. Wulzer and M. Zanetti, *JHEP* **1708**, 074 (2017) [arXiv:1704.00736 [hep-ph]].
 - [8] R. C. Cotta, J. L. Hewett, M. P. Le and T. G. Rizzo, *Phys. Rev. D* **88**, 116009 (2013) [arXiv:1210.0525 [hep-ph]]. L. M. Carpenter, A. Nelson, C. Shimmin, T. M. P. Tait and D. Whiteson, *Phys. Rev. D* **87**, no. 7, 074005 (2013) [arXiv:1212.3352 [hep-ex]]. A. Freitas and S. Westhoff, *JHEP* **1410**, 116 (2014) [arXiv:1408.1959 [hep-ph]]. A. Alves and K. Sinha, *Phys. Rev. D* **92**, no. 11, 115013 (2015) [arXiv:1507.08294 [hep-ph]].
 - [9] A. Crivellin, U. Haisch and A. Hibbs, *Phys. Rev. D* **91**, 074028 (2015) [arXiv:1501.00907 [hep-ph]].
 - [10] A. M. Sirunyan *et al.* [CMS Collaboration], *JHEP* **1710** (2017) 073 [arXiv:1706.03794 [hep-ex]]. M. Aaboud *et al.* [ATLAS Collaboration], *Eur. Phys. J. C* **77**, no. 6, 393 (2017) [arXiv:1704.03848 [hep-ex]].
 - [11] Z. H. Yu, X. J. Bi, Q. S. Yan and P. F. Yin, *Phys. Rev. D* **90**, no. 5, 055010 (2014) [arXiv:1404.6990 [hep-ph]].
 - [12] A. Rajaraman, T. M. P. Tait and A. M. Wijangco, *Phys. Dark Univ.* **2**, 17 (2013) [arXiv:1211.7061 [hep-ph]].
 - [13] J. Y. Chen, E. W. Kolb and L. T. Wang, *Phys. Dark Univ.* **2**, 200 (2013) [arXiv:1305.0021 [hep-ph]].
 - [14] V. Barger, W. Y. Keung and D. Marfatia, *Phys. Lett. B* **696**, 74 (2011) [arXiv:1007.4345 [hep-ph]].
 - [15] B. Geytenbeek, S. Rao, P. Scott, A. Serenelli, A. C. Vincent, M. White and A. G. Williams, *JCAP* **1703**, 029 (2017) [arXiv:1610.06737 [hep-ph]].
 - [16] C. M. Ho and R. J. Scherrer, *Phys. Lett. B* **722**, 341 (2013) [arXiv:1211.0503 [hep-ph]]. Y. Gao, C. M. Ho and R. J. Scherrer, *Phys. Rev. D* **89** (2014) no.4, 045006 [arXiv:1311.5630 [hep-ph]].
 - [17] T. Banks, J. F. Fortin and S. Thomas, arXiv:1007.5515 [hep-ph].
 - [18] E. Del Nobile, G. B. Gelmini, P. Gondolo and J. H. Huh, *JCAP* **1406**, 002 (2014) [arXiv:1401.4508 [hep-ph]].
 - [19] [LEP and ALEPH and DELPHI and L3 and OPAL Collaborations and Line Shape Sub-Group of the LEP Electroweak Working Group], hep-ex/0101027.

- [20] Z. H. Yu, Q. S. Yan and P. F. Yin, Phys. Rev. D **88**, no. 7, 075015 (2013) [arXiv:1307.5740 [hep-ph]].
- [21] A. Belyaev, N. D. Christensen and A. Pukhov, Comput. Phys. Commun. **184**, 1729 (2013) [arXiv:1207.6082 [hep-ph]].
- [22] CEPC-SPPC Study Group, IHEP-CEPC-DR-2015-01, IHEP-TH-2015-01, IHEP-EP-2015-01.
- [23] CEPC-SPPC Study Group, IHEP-CEPC-DR-2015-01, IHEP-AC-2015-01.
- [24] N. Weiner and I. Yavin, Phys. Rev. D **86**, 075021 (2012) [arXiv:1206.2910 [hep-ph]].
- [25] M. T. Frandsen, U. Haisch, F. Kahlhoefer, P. Mertsch and K. Schmidt-Hoberg, JCAP **1210**, 033 (2012) [arXiv:1207.3971 [hep-ph]].
- [26] R. Agnese *et al.* [SuperCDMS Collaboration], Phys. Rev. Lett. **112**, no. 24, 241302 (2014) [arXiv:1402.7137 [hep-ex]].
- [27] L. T. Yang *et al.* [CDEX Collaboration], arXiv:1710.06650 [hep-ex].
- [28] R. Agnese *et al.* [SuperCDMS Collaboration], Phys. Rev. Lett. **116**, no. 7, 071301 (2016) [arXiv:1509.02448 [astro-ph.CO]].
- [29] E. Aprile *et al.* [XENON Collaboration], Phys. Rev. Lett. **119**, no. 18, 181301 (2017) [arXiv:1705.06655 [astro-ph.CO]].
- [30] D. S. Akerib *et al.* [LUX Collaboration], Phys. Rev. Lett. **118**, no. 2, 021303 (2017) [arXiv:1608.07648 [astro-ph.CO]].
- [31] X. Cui *et al.* [PandaX-II Collaboration], Phys. Rev. Lett. **119**, no. 18, 181302 (2017) [arXiv:1708.06917 [astro-ph.CO]].
- [32] M. Ackermann *et al.* [Fermi-LAT Collaboration], Phys. Rev. D **91**, no. 12, 122002 (2015) [arXiv:1506.00013 [astro-ph.HE]].
- [33] D. M. Asner *et al.*, arXiv:1310.0763 [hep-ph].